Photoluminescence and Infrared Properties of α-Al_2O_3 Nanowires and Nanobelts

X. S. Peng,* L. D. Zhang, G. W. Meng, X. F. Wang, Y. W. Wang, C. Z. Wang, and G. S. Wu

Institute of Solid State Physics, Chinese Academy of Sciences, Hefei 230031, P. R. China

Received: April 28, 2002; In Final Form: August 22, 2002

α-Al_2O_3 nanowires and nanobelts have been successfully synthesized from Al pieces and SiO_2 nanoparticles at 1200 °C and 1150 °C, respectively, in a flowing Ar atmosphere. The α-Al_2O_3 nanowires are uniform with diameters of 20−70 nm and lengths of 15−25 μm, and the nanobelts are several to tens of micrometers long, with width of 0.1−1 μm and thickness of 10−50 nm. The growth of the nanowires is controlled by a vapor−liquid−solid (VLS) growth mechanism, while the growth of the nanobelts may be due to a vapor−solid (VS) process. Infrared spectra of these nanostructures are different from that of the bulk α-Al_2O_3. Photoluminescence (PL) measurements under excitation at about 255 nm show that the nanowires and nanobelts have emission peaks at 394 and 392 nm, respectively. On the basis of the discussion of the thermal annealing in different atmospheres such as O_2 and H_2 on the behaviors of the PL spectra, we suggest that optical transitions in oxygen-related defects, F^+ (oxygen vacancy with one electron) centers, are responsible for the observed emission.

Introduction

The novel properties of one-dimensional (1D) nanostructured materials have attracted extensive interest over the decade as a result of their great potential for addressing some basic issues about dimensionality and size-confined transport phenomena, as well as applications in nanosensors,[1,2] logic gates, and computations.[3,4] Aside from nanotubes,[4] various nanowires (nanorods) have been fabricated by using various methods such as laser ablation,[5] templating,[6] arc discharge,[7] vapor-phase transport,[8] and solution method.[9] Recently, much attention has been paid to the preparation of oxide nanostructures for their interesting optical and electronical properties. Nanowires of several oxides such as MgO,[10] SiO_2,[11] Ga_2O_3,[7] GeO_2,[12] ZnO,[13] In_2O_3,[14] and oxide nanobelts such as Ga_2O_3, In_2O_3, CdO, ZnO,[15] have been successfully synthesized. Owing to their brittleness, oxide ceramics have been regarded as materials of modest performance, especially under tension or bending conditions. In contrast to metals or polymers, however, the thermal stability of ceramics above 700 °C makes them suitable materials for high-temperature applications. Microstructural design is critical in order to obtain reliable ceramic materials. Such materials are usually called "advanced ceramics". Recently, inorganic nanostructured materials are being widely used to improve the toughness of advanced ceramics. The use of Al_2O_3 polycrystalline fibers and whiskers (short single crystals) as strengtheners in high-temperature compositions is of great interest owing to their high elastic modulus and their thermal and chemical stability. [16]

An enormous effort has been made to obtain alumina and aluminosilicate fibers with a high Al_2O_3 content.[17] Recently, Al_2O_3 nanowires with impurity Si nanowires have been synthesized through an in-situ catalytic growth mechanism using Fe as catalyst.[18] In the present work, we have successfully synthesized α-Al_2O_3 nanowires and nanobelts by using silica nanoparticles and Al pieces without any other catalyst at 1200 °C and 1150 °C, respectively, in a fast heating process. We also studied the PL and infrared (IR) properties of the as-synthesized α-Al_2O_3 nanowires and nanobelts, and found that the nanowires and nanobelts have different optical properties. The PL intensity of the nanobelts is stronger than that of the nanowires, and as for the infrared properties of the nanowires have two peaks shifted blue and one peak shifted red compared with that of the nanobelts. According to the PL spectra of the samples annealed in different atmospheres such as O_2 and H_2 at 600 °C, we suggest that optical transitions in oxygen-related defects, F^+ (oxygen vacancy with one electron) centers, are responsible for the observed emission.

Experimental Section

Ultrahigh purity (99.999%) aluminum and pure SiO_2 nanoparticles were used as starting materials. The apparatus used was a horizontal electronic resistance furnace heated by silicon−carbon rods. A shallow bed of SiO_2 nanoparticles was placed in a small ceramic boat. For the preparation of nanowires, small pieces of Al ($10 \times 20 \times 0.3$ mm^3) were put above SiO_2 nanoparticles. Then the system was rapidly heated to 1200 °C, and kept at this temperature for 2 h. But for producing nanobelts, the pieces of Al were laid on the shallow bed of SiO_2 nanoparticles and covered with another thin layer of SiO_2 nanoparticles, and then heated to 1150 °C and kept for 2 h. A constant flow of Ar (99.99%) at a flow rate of 200 sccm was maintained during the overall experiment. After the system had cooled to room temperature, a large piece of transparent, wool-like product was collected from the inner wall of the ceramic boat at the downstream end. The synthesized products were characterized by X-ray diffraction (XRD) (PW 1710 instrument with Cu Kα radiation), scanning electron microscopy (SEM) (JEOL JSM 6700F), high-resolution transmission electron microscopy (HRTEM) (JEOL 2010, operated at 200 kV) equipped with energy-dispersive X-ray fluorescence (EDX) (EDAX, DX-4). For SEM observation, the product was pasted on the Al substrate by carbon conducting paste. Specimens for TEM and HRTEM investigation were briefly ultrasonicated in

* Author to whom correspondence should be addressed: Fax: +86-551-5591434. E-mail: zyzhao@mail.issp.ac.cn.

10.1021/jp026028+ CCC: $22.00
Published on Web 10/08/2002

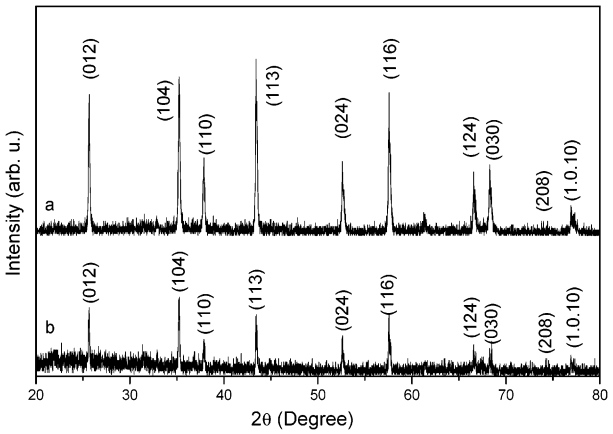

Figure 1. XRD patterns of the products: (a) nanowires, and (b) nanobelts.

ethanol, and then a drop of suspension was placed on a holey copper grid with carbon film. PL and photoluminescence excitation (PLE) spectra were obtained using a Hitachi 850-fluorescence spectrophotometer with a filter at 310 nm and Xe lamp at room temperature. Infrared spectra were recorded at room temperature on a Nicolet Magna-750 Fourier transform infrared spectrometer on samples palletized with KBr powder.

Results and Discussions

1. Structural Characterization. Figure 1 shows the XRD patterns of the nanowires (curve a) and nanobelts (curve b). All the diffraction peaks can be indexed to those of the bulk α-Al_2O_3.[19] It is clear that the nanowires and the nanobelts have the same phase.

Figure 2a and b show the representative SEM images of the as-synthesized Al_2O_3 nanowires with diameters of 20−70 nm and lengths of 15−25 μm. Figure 2c shows the morphology of the nanobelts with width of 0.1−1 μm, thickness of 10−50 nm, and length of several to tens of micrometers. It can be observed that when Al pieces were not covered with the SiO_2 nanoparticles (as described in the Experimental Section), the product was nanowires with a very small number of nanobelts (Figure 1a). Figure 2b shows a high-magnification SEM image of a single nanowire with a nanoparticle at the end. This result indicates that the growth mechanism of the nanowires is through a vapor−liquid−solid (VLS) method. The corresponding EDX analyses taken from the particles (curve 1) and the stem (curve 2), respectively, are shown in Figure 2d. All the results indicate that the nanoparticles are composed of Si 2.31 atom %, Al 39.92 atom %, and O 58.77 atom %, whereas the stem of the nanowires consists of Al 41.24 atom % and O 58.76 atom %, in good agreement with the corresponding ratio of bulk Al_2O_3 (Al:O = 2:3). Nanobelts were predominately found at the particular locations where the Al pieces were in contact with the SiO_2 nanoparticle bed. It is likely that special features on the interface promote nanobelt formation. This result indicates that if Al pieces were covered with a thin layer of SiO_2 nanoparticles, nanobelts would be preferentially obtained. Using Al pieces covered with SiO_2 nanoparticles as starting materials, we have successfully fabricated large quantities of nanobelts (Figure 2c). The corresponding EDX analysis (curve 3 in Figure 2d) indicates that the nanobelts are composed of Al 39.12 atom % and O 61.88 atom %, in good agreement with the corresponding ratio of bulk Al_2O_3 (Al:O = 2:3).

Figure 3a is a TEM image of a single Al_2O_3 nanowire with a diameter of 20 nm, Figure 3b is the corresponding lattice-

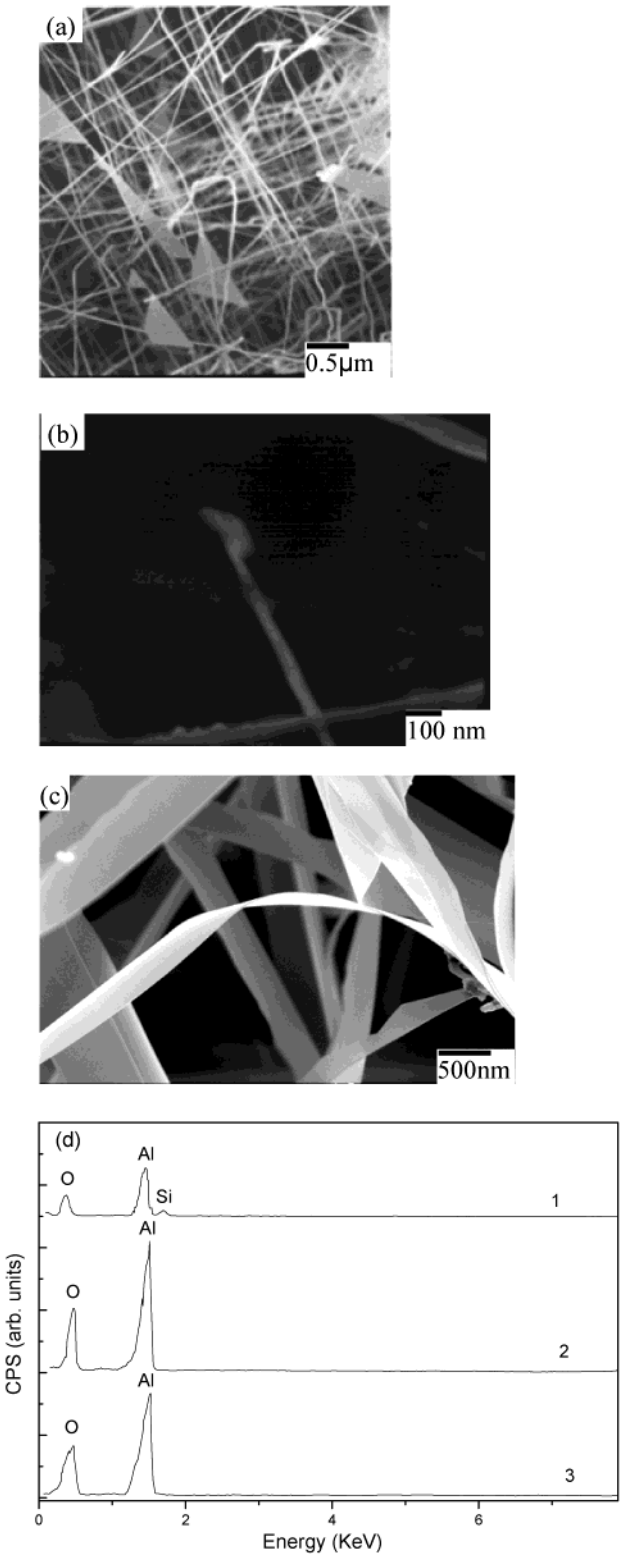

Figure 2. SEM images of (a) the as-synthesized Al_2O_3 nanowires, (b) a single nanowire with a nanoparticle at the end, and (c) nanobelts. (d) EDX analyses taken from the nanoparticles (curve 1) and the stem of the nanowire (curve 2) and one nanobelt (curve 3).

resolved TEM image and SAED pattern (insert) recorded perpendicularly to the long axis of the nanowire, revealing that the Al_2O_3 nanowire is single-crystalline with an inter-planar spacing of 0.432 nm, in agreement with the *d* value of the (003) planes of the α-Al_2O_3 crystal with growth along the ⟨003⟩ direction.

Figure 4a shows a typical TEM image of a very thin nanobelt

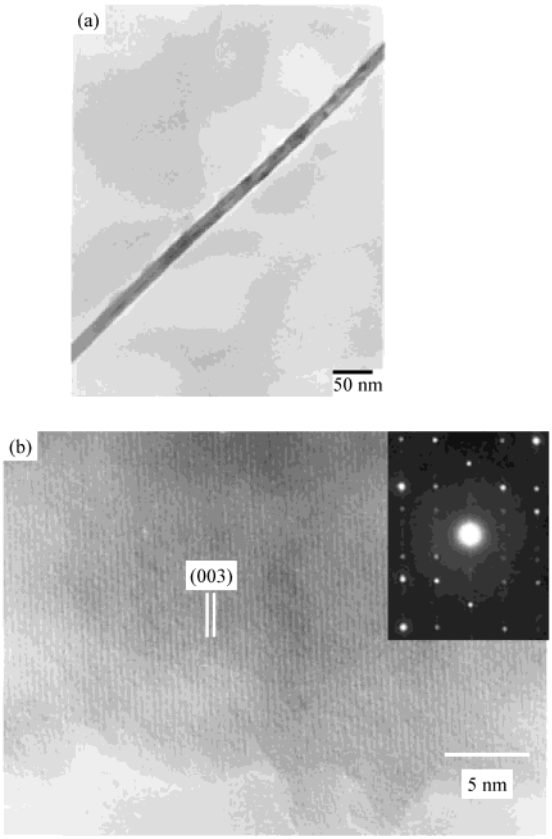

Figure 3. (a) A TEM image of a representative single nanowire. (b) The corresponding HRTEM image and SAED pattern (the insert in it) of the nanowire.

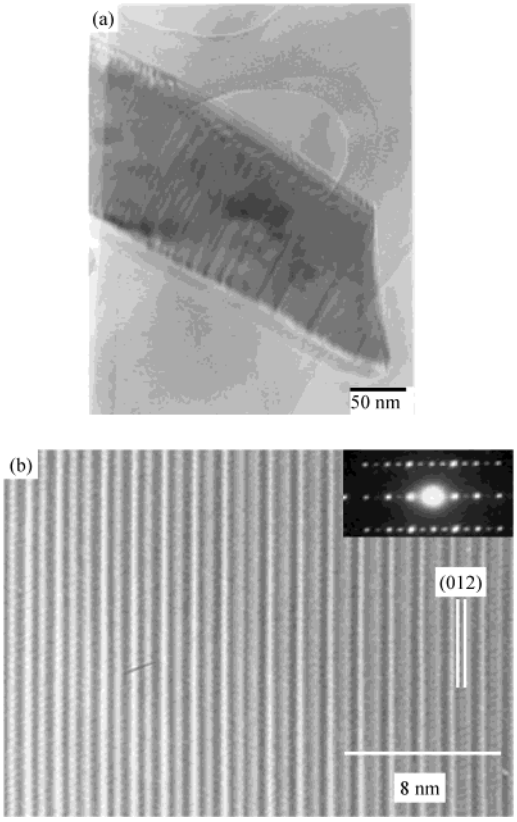

Figure 4. (a) A typical TEM image of a very thin nanobelt with two parallel flat faces. (b) The corresponding HRTEM image and SAED pattern recorded from the nanobelts.

(about 20 nm) with two parallel flat faces and is very thin. Furthermore, the corresponding HRTEM image (Figure 4b) and SAED pattern (the insert in Figure 4b) reveal that the nanobelts are single-crystalline and the crystal lattice fringes are spaced 0.347 nm apart, in agreement with the *d* value of the (012) planes of the α-Al_2O_3 crystal with growth along the ⟨012⟩ direction.

From Figure 3b and Figure 4b, it can be found that both the Al_2O_3 nanowires and the nanobelts have the same α-Al_2O_3 phase, in good agreement with the XRD results (Figure 1).

2. Infrared Properties. Figure 5 shows the IR spectra of Al_2O_3 micro-powders with diameters of 5−10 μm annealed at 1200 °C (curve a), nanowires (curve b), and nanobelts (curve c), respectively. The corresponding IR absorption peaks are marked as A, B, and C.

It can be seen that all the peaks of the nanowires and nanobelts are similar to those of Al_2O_3 micro-powders. However, peak A is blue-shifted from 447.41 (micro-powders) to 449.34 (nanowires) and 451.27 cm^{-1} (nanobelts); peak B is red-shifted from 592.05 (micro-powders) to 586.26 (nanowires) and 582.26 cm^{-1} (nanobelts); and peak C is first red-shifted from 638.33 (micro-powders) to 636.4 (nanowires) and second blue-shifted to 638.35 cm^{-1} (nanobelts). The blue-shift is possibly due to the size-confinement, and the red-shift may be owing to the suspending bonds on the surface of the nanostructures. Previous investigations on the IR properties of α-Al_2O_3 nanocrystals demonstrate that the three corresponding IR peaks for grain sizes of 8, 15, and 35 nm are 639.7, 583.5, and 456.5 cm^{-1}; 635, 592, and 453 cm^{-1}; 639.7, 583.7, and 449.6 cm^{-1}, respectively.[20] Therefore, it can be seen that not only nanocrystal but also the present Al_2O_3 nanowires and nanobelts have IR properties similar to that of α-Al_2O_3 micro-powders.

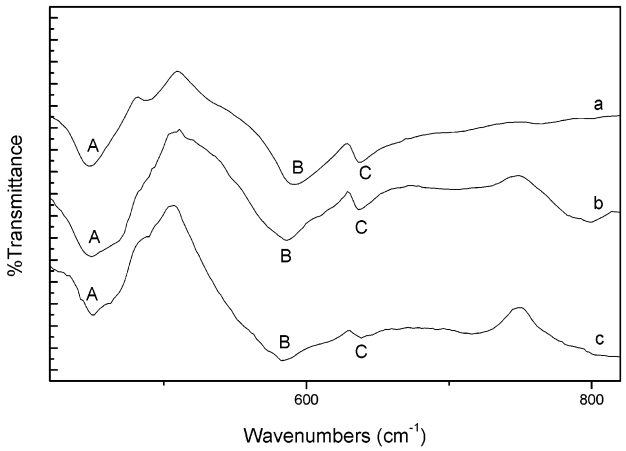

Figure 5. The IR spectra of Al_2O_3 (a) micro-powders with diameters of 1−10 μm annealed at 1200 °C, (b) nanowires, and (c) nanobelts, respectively. The corresponding IR absorption peaks are marked as A, B, and C.

3. Photoluminescence Properties. Figure 6 shows PL (solid line) and PLE (dashed line) spectra of nanowires (curve a) and nanobelts (curve b), respectively. When the nanowires were excited at 255.6 nm, there exists a strong PL peak at 394 nm (solid line, curve a). The PL spectrum of nanobelts (solid line, curve b) shows a peak at 392 nm when excited at 255 nm. The corresponding PLE spectra for the observed PL peaks were showed in Figure 6 (the dashed line). It is obvious that for PL peaks (394 or 392 nm), sharp PLE peaks at 255 nm were observed. But for the Al_2O_3 micro-powders (annealed at 1200 °C), there is no PL emission.

What are the origins of these PL peaks? Curves a, c, and d in Figure 7 show the PL spectra of the Al_2O_3 nanobelts annealed

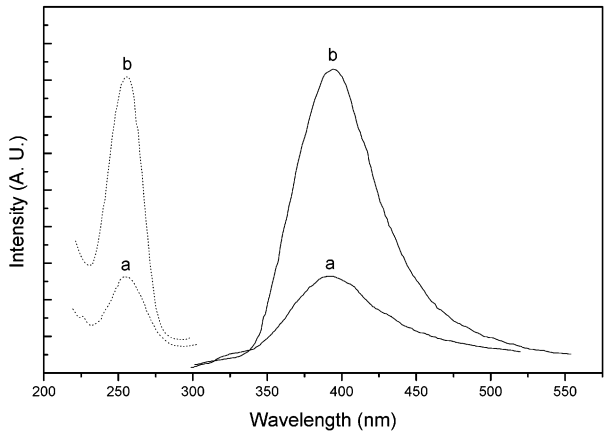

Figure 6. PL (solid line) and PLE (dashed line) spectra of Al_2O_3 nanowires (a) and nanobelts (b), respectively.

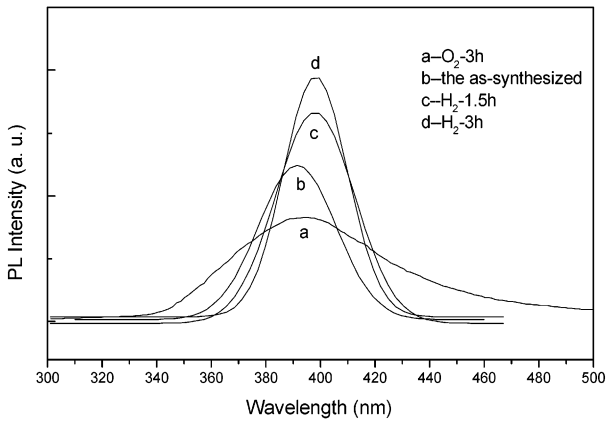

Figure 7. PL spectra of (a) the Al_2O_3 nanobelts annealed at 600 °C in O_2 for 3 h; (b) the as-synthesized; (c) and (d) after being annealed at 600 °C in H_2 for 1.5 and 3 h, respectively; measured with an excitation of the 255 nm line of a Xe lamp.

at 600 °C in O_2 for 3 h, H_2 for 1.5 and 3 h, respectively, measured with an excitation of the 255 nm line of a Xe lamp. For comparison, the PL spectrum of the as-synthesized Al_2O_3 nanobelts is also presented as curve b in Figure 7. Obviously, all the spectra show one similar strong PL peak. In comparison with that of the as-synthesized Al_2O_3 nanobelts (curve b in Figure 7), the intensity of the PL band decreases after being annealed in oxygen (curve a in Figure 7), but increases after being annealed in H_2 with an increase in the annealing time (curve c and d in Figure 7). This result implies that the radiative centers leading to the observed PL are oxygen-deficient. It has been reported that color centers (F_2, F_2^+, F_2^{2+}, F, and F^+) related to oxygen vacancies can originate optical absorption bands and corresponding luminescence bands in ultraviolet or violet.[21−23] An obvious feature of those luminescence bands from F_2, F_2^+, and F_2^{2+} centers is that the PL peak intensity and position change with the ultraviolet illumination time, because these defect centers could be ionized under the illumination of ultraviolet light to transfer to each other.[22−23] However, in our experiment, the PL peak intensity and position are hardly changed with the illumination time. For the F center, it should have a strong PLE band at 207 nm (6.05 eV),[24] but we have not observed the 207 nm PLE band. Therefore, the PL bands in our experiment are not generated from F_2, F_2^+, and F_2^{2+} centers. It has been reported that F^+ (oxygen vacancies with one electron) centers in α-Al_2O_3 cause ultraviolet or violet PL bands[24−26] and blue PL bands in porous amorphous anodic alumina films.[27,28] We believe that the PL peaks observed in our experiment are intimately associated with the F^+ center. In the present experiment, the high aspect ratio and peculiar morphologies of Al_2O_3 nanowires and nanobelts should also favor the existence of oxygen vacancies.[14] The PL and PLE intensities of nanobelts are stronger than those of nanowires. It may be due to more oxygen vacancies in nanobelts for their large surface favoring to generate suspending bonds. As for the decrease of the PL intensity after the sample is annealed in oxygen, it is mainly due to the reduction of the oxygen vacancy density. But the increase of the PL intensities after the samples are annealed in hydrogen is principally attributed to the increase of the oxygen vacancy density.

The peak positions slightly exhibit red-shift from curve a to curve d, Figure 7. That is to say, the PL bands present red-shift with the increase of oxygen vacancies. It has been reported that with the increase of oxygen vacancies, the band gap of the silica becomes narrow dramatically.[29] Therefore, it is supposed that the increase of oxygen vacancies in our samples may induce the band gap of alumina to become narrow. Since the energy levels of F^+ centers are located in the band gap of alumina, with the increase of oxygen vacancies the decreasing of the band gap of alumina will induce the spacing of the energy levels of F^+ centers to become narrow. It will lead the PL band, which originates from the electronic transitions between the energy levels of the F^+ centers, to move toward the long wavelength (red-shift).[27] Because the α-Al_2O_3 obtained in our experiment is the most stable structure among the phases of Al_2O_3, the emission position does not change with the annealing temperature in Ar atmosphere.

Growth Mechanism

The vapor−liquid−solid (VLS) and vapor−solid (VS) crystal growth mechanism have been widely used for the growth of elemental semiconductor nanowires such as Si[5] and oxide semiconductor nanowires. [14] To understand the growth mechanism of these Al_2O_3 nanowires and nanobelts, the following reactions may involved:

$$4Al(g) + SiO_2(s) \rightarrow 2Al_2O(g) + Si(s,l) \quad (1)$$

$$2Al(g) + SiO_2 \rightarrow Al_2O(g) + SiO(g) \quad (2)$$

$$Al_2O(g) + 2SiO(g) \rightarrow Al_2O_3(s) + Si(l) \quad (3)$$

For nanowires**,** there exists a nanoparticle at the end of the nanowire (Figure 2b). The different compositions of the stem and the nanoparticle reveal that the presence of Si in the nanoparticle at the end of the nanowire represents strong evidence for a growth process dominated by a VLS mechanism. In the Si−SiO system, a eutectic alloy/mixture can be generated (as proposed by Sosman[30]). The compositions needed for liquid can appear and the gases (Al(g), Al_2O(g), and SiO(g)) can reach and come into the liquid. When the Al_2O_3 formed and becomes supersaturated in the liquid Si−SiO, Al_2O_3 nanowires will be produced.

As for the nanobelts predominately found at the particular locations where the Al pieces were in contact with the SiO_2 nanoparticle bed, it is likely that special features at this interface promote nanobelt formation. At this interface, the yield ratio of vapors should be higher than that for the formation of nanowires, resulting in the formation of nanobelts. In addition, for the nanobelts without nanoparticles at their ends, it is difficult to elucidate how VLS deposition can form a crystal much wider than the drop diameter, and why drops do not appear consis-

tently. Therefore, the mechanism for the nanobelt growth is probably through a VS process similar to that reported for Al_2O_3 micro-ribbon.[29]

Conclusion

In summary, we have described a novel method for the synthesis of α-Al_2O_3 nanowires and nanobelts. The emission peaks at 394 nm from α-Al_2O_3 nanowires and 392 nm from nanobelts may be attributed to oxygen vacancies. According to the PL spectra of the samples annealed in different atmospheres such as O_2 and H_2 at 600 °C, we suggest that optical transitions in oxygen-related defects, F^+ (oxygen vacancy with one electron) centers, are responsible for the observed emission. These α-Al_2O_3 nanostructures may possibly be used as reinforcement in composites. Especially, the nanobelts, which are flat and therefore have high specific surface area, which is an important feature for low-cost layer-forming elements in composites. Such coatings are likely to improve the tribological properties of composites, and also their resistance to oxidation and to acids. A further common use of single-layer nano-thin films is in the production of antireflection coatings.

Acknowledgment. This work was supported by the Key Project of National Fundamental Research and the Natural Science Foundation of China (Grant No. 19974055).

References and Notes

(1) Cui, Y.; Wei, Q. Q.; Park, H.; Lieber, C. M. *Science* **2001**, *293*, 1289.
(2) Favier, F.; Walter, E. C.; Zach, M. P.; Benter, T.; Penner, R. M. *Science* **2001**, *293*, 2227.
(3) Huang, Y.; Duan, X. F.; Cui, Y.; Lauhon, L. J.; Kim, K.-H.; Lieber, C. M. *Science* **2001**, *294*, 1313.
(4) Bachtold, A.; Hadley, P.; Nakanishi, T.; Dekker: C. *Science* **2001**, *294*, 1317.
(5) Duan, X. F.; Lieber, C. M. *Adv. Mater.* **2000**, *12*, 298.
(6) Li, Y.; Meng, G. W.; Zhang, L. D.; Phillipp, F. *Appl. Phys. Lett.* **2000**, *76*, 2011.
(7) Choi, Y. C.; Kim, W. S.; Park, Y. S.; Lee, S. M.; Bae, D. J.; Lee, Y. H.; Park, G. S.; Choi, W. B.; Lee, N. S.; Kim, J. M. *Adv. Mater.* **2000**, *12*, 746.
(8) Wu, Y.; Yang, P. D. *Chem. Mater.* **2000**, *12*, 605.
(9) Trentlet, T. J.; Hickmans, K. M.; Goel, S. C.; Viano, A. M.; Gibbons, P. C.; Buhro, W. E. *Science* **1995**, *270*, 1791.
(10) Yang, P. D.; Lieber, C. M. *Science* **1996**, *273*, 1836.
(11) Wang, Z. L.; Gao, R. P.; Gole, J. L.; Stout, J. D. *Adv. Mater.* **2000**, *12*, 1938.
(12) Bai, Z. G.; Yu, D. P.; Zhang, H. Z.; Ding,; Y.; Gai, X. Z.; Hang, Q. L.; Xong, G. C.; Feng, S. Q. *Chem. Phys. Lett.* **1999**, *303*, 311.
(13) Hang, M. H.; Wu, Y.; Feick, H.; Tran, N.; Weber, E.; Yang, P. D. *Adv. Mater.* **2001**, *13*, 113.
(14) Liang, C. H.; Meng, G. W.; Lei, Y.; Phillipp, F.; Zhang, L. D. *Adv. Mater.* **2001**, *13*, 1330.
(15) Pan, Z. W.; Dai, Z. R.; Wang, Z. L. *Science* **2001**, *291*, 1947.
(16) Das, G. *Ceram. Eng. Sci. Proc.* **1995**, *16*, 977.
(17) Cooke, T. F. *J. Am. Ceram. Soc.* **1991**, *74*, 2959.
(18) Tang, C. C.; Fan, S. S.; Li, P.; Chapelle, M. L.; Dang, H. Y. *J. Crystal Growth* **2001**, *224*, 117.
(19) JCPDS: 10−173.
(20) Mo, C. M.; Yuan, Z. H.; Zhang, L. D. *Nanostruct. Mater.* **1993**, *2*, 47.
(21) Levy, P. W. *Phys. Rev.* **1961**, *123*, 1226.
(22) Ghamdi, A. Al; Townsend, P. *Nucl. Instrum. Methods Phys. Rev., Sect. B* **1990**, *46*, 133.
(23) Pogatshnik, G. J.; Chen, Y.; Evans, B. D. *IEEE Trans. Nucl. Sci.* **1987,** *NS-34*, 1709.
(24) Evans, D.; Stapelbroek, M. *Phys. Rev. B* **1978**, *18*, 7089.
(25) Wu, J. H.; Wu, X. L.; Tang, N.; Mei, Y. F.; Bao, X. M. *Appl. Phys. A* **2001**, *72*, 735.
(26) Chen, W.; Tang, H. G.; Wang, Y. X.; Yin, S. T. *Appl. Phys. Lett.* **1995**, *67*, 317.
(27) Du, Y.; Cai, W. L.; Mo, C. M.; Chen, J.; Zhang, L. D.; Zhu, X. G. *Appl. Phys. Lett.* **1999**, *74*, 2951.
(28) Chen, J.; Cai, W. L.; Mo, J. M. *J. Inorg. Mater.* **2001**, *16*, 677.
(29) Philipp, H. R. *J. Phys. Chem. Solids* **1971**, *32*, 1935.
(30) Sosman, R. B. *Trans. Br. Ceram. Soc.* **1955**, *54*, 655.